Executive Summary of the Thesis

Synthesis and Characterization of Zinc Manganite Thin Films for Zinc-Ion Battery Applications

Laurea Magistrale in Nuclear Engineering - Ingegneria Nucleare

Author: Marco Olivieri

Advisor: Prof. Andrea Li Bassi

Co-advisor: Dr. Andrea Macrelli

Academic year: 2021-2022

1. Introduction

The interest in energy storage systems has been growing. Society wants to progress toward an increasingly sustainable future, and this drives the battery market; on the other hand, it also requires batteries to be more sustainable, safe, and disposed of in an environmentally friendly manner. Current lithium-ion batteries are struggling to keep up with these demands. An electric battery is a system for the storage of electric energy consisting of one or more electrochemical cells with external connections for powering electrical devices. Considering one electrochemical cell, its main components are three: the anode (negative electrode), the cathode (positive electrode), and the electrolyte. The most common and widely used rechargeable battery is the lithium-ion battery (LIB). Traditionally, LIBs consist of a graphite anode (LiC_6), a lithiated metal oxide as the cathode (like $LiCoO_2$), and, finally, an organic liquid as the electrolyte. The lithium ions migrate back and forth during charging and discharging and are intercalated into the active materials of electrodes. In LIBs, typical cathode materials contain cobalt, which is one of the critical steps in the supply chain. Cobalt is rare, expensive, and toxic. An-other major limitation is the organic electrolyte, which is difficult to recycle and poses safety concerns due to flammability. In addition, lithium metal is the ideal anode material, but it is highly unstable. These limitations can be overcome by zinc-ion batteries.

2. Zinc-ion batteries and ZMO cathode

Zinc-ion batteries (ZIBs) are a promising storage technology, particularly for stationary storage applications. Non-toxic and abundant materials are used, and these batteries can provide more specific power than LIBs. The key advantages of ZIBs are:

1. The availability of zinc: Zn is among the most common elements in the earth's crust and it is present on all continents and produced worldwide at affordable prices. In addition, the manufacturing and recycling technology for Zn is well-established;

2. The use of an aqueous electrolyte that is low cost, non-flammable, non-toxic, safe, highly-conductive, and versatile for design modifications;
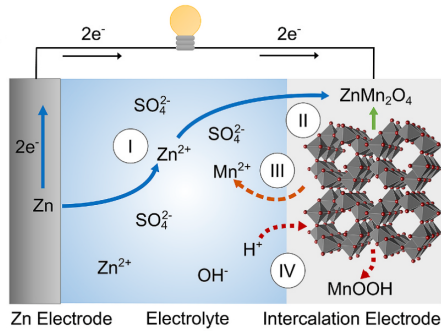
3. The stability of metallic zinc in the aqueous

Figure 1: Zinc-ion battery scheme taken from [1].

electrolyte, which allows its use in the battery without resorting to zinc compounds and thus leading to a higher theoretical capacity.

In Figure 1, the scheme of the ZIB is presented. The anode is composed of metallic zinc, and the most common salt used for aqueous near-neutral electrolyte is $ZnSO_4$. The working principle is the shuttle mechanism, where the charge transfer is due to the migration of Zn^{2+} from the anode to the cathode. During discharge, when the zinc-ion reaches the cathode, it intercalates accompanied by the reduction reaction of the host cations. The development of aqueous ZIBs is nowadays mainly aimed at finding compatible cathodes and studying the associated electrochemical mechanisms. Electronic and ionic transport properties and reaction kinetics of the cathode affect the specific energy and power of the ZIB. In the end, cathode stability and integrity over the cycles are major factors in the cycling stability of the battery itself. Manganese dioxide (MnO_2) materials are particularly desirable candidates for large-scale systems due to their abundance, easy processing, ecofriendly nature, multiple oxidation states of Mn, and low cost. The theoretical specific capacity for manganese oxide is 308 Ah/kg, with one electron transfer per formula unit. In general, the manganese oxide active materials undergo complex structural transformations from tunnel-like to spinel-like and layered phases on discharging. These transitions of structure and phase, along with Mn^{2+} dissolution, lead to poor cyclability. It appears that most of MnO_x undergo irreversible phase transformation into spinel $ZnMn_2O_4$ after multiple charge/discharge cycles. The zinc manganite $ZnMn_2O_4$ (ZMO) material is recently studied as one of the possible cathodes for ZIBs. Its structure is composed of tetrahedral and octahedral sites, partially occupied by divalent cations and trivalent cations, respectively. Unfortunately, although ZMO as cathode material has a theoretical specific capacity of 224 Ah/kg[2], experiments show that stoichiometric bulk ZMO is unfit for Zn^{2+} insertion due to the high electrostatic repulsion among Zn ions with the lattice cations.[3] By acting on the stoichiometry and morphology of the material, good electrochemical performances can be obtained. There are different strategies to enhance the ZMO electrochemical performance, among them:

1. Introduction of vacancies in the structure.
   The introduction of vacancies removing some cations (i.e. Mn^{3+}) relaxes the electrostatic condition of the structure, reducing the repulsion and improving the transfer kinetics.

2. Nanostructured ZMO and morphology modifications.
   Changing the morphology allows having more active sites in the material, increasing the conductivity (due to the shorter path) and the diffusion. Moreover, reducing the crystal size or developing some peculiar morphologies can alleviate the strain on the structure due to volume changes during electrochemical cycles.[3]

The ZMO electrochemical mechanism is not yet clear. Although the insertion/extraction of zinc ions is one of the most accredited mechanisms[2], there are also studies reporting on the mechanism of H^+/Zn^{2+} co-insertion/extraction, intercalation of H^+ only, and dissolution/deposition reactions [4]. The objectives of this thesis are:

1. The production of nanostructured ZMO thin films using Pulsed Laser Deposition with the aid of different gas atmospheres during deposition.

2. The characterization of the produced materials by different techniques and the correlation of the material properties to the parameters used in the synthesis process.

3. The conducting of some preliminary electrochemical tests aimed at observing the

material response and at characterizing the material changes in the aged samples.

3. Synthesis and structural characterization of as-deposited ZMO films

In this thesis, I chose to produce ZMO thin films using the Pulsed Laser Deposition (PLD) technique. These films were then characterized via Scanning Electron Microscopy (SEM), Energy Dispersive X-ray Spectroscopy (EDXS), and Raman spectroscopy. Most of the samples were deposited using PLD in vacuum or oxygen atmosphere using a laser fluence of $\sim$3.8 J/cm^2 on silicon substrates. Other deposition parameters were used for some specific tests. For example, I deposited films with different laser fluences to relate this parameter to the deposition rate and to the films' morphology, showing that, as the fluence increases, the film morphology becomes more and more compact. For the next analysis, the fluence was maintained constant and only the oxygen deposition pressure was varied (from vacuum to 150 Pa). SEM images acquired show a more compact morphology for depositions in vacuum and at oxygen pressures up to 70 Pa, while at higher deposition pressures (100 Pa and 150 Pa) the film appears to be formed by forest-like nanostructures with extensive nano-porosity (Figure 2). The increase of film porosity from vacuum to 150 Pa of oxygen is accompanied by a decrease of density and increase of surface area. Characterization of samples deposited in vacuum and at various oxygen pressures continues with stoichiometry analysis measured by EDXS. Figure 3 shows the percentage trends of the elemental compositions of the films. Films deposited in vacuum or at low O_2 pressures (< 10 Pa) are poor in oxygen and have a higher content of Zn and Mn. The trend as a function of the pressure exhibits a plateau where the stoichiometry stabilizes and becomes almost constant irrespective of oxygen deposition pressures. Finally, the Raman spectra of as-deposited ZMO films produced at various oxygen pressures and 3.8 J/cm^2 fluence are shown in Figure 4. All the spectra consist of broad bands centered around 600-650 cm^{-1}, indicating an amorphous nature of the film. It can be seen that the band of the film deposited in 1 Pa oxygen differs from the

(a)

(b)
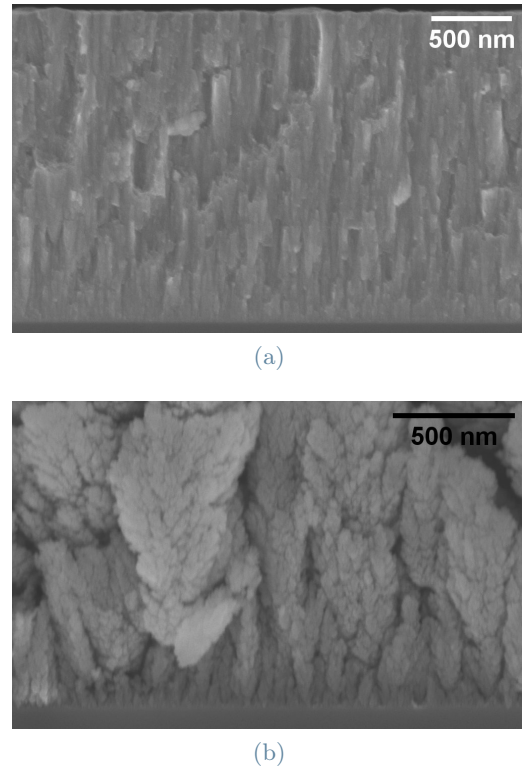
Figure 2: SEM images of as-deposited ZMO films produced at 30 and 150 Pa of oxygen, respectively, and with 3.8 J/cm^2 laser fluence.
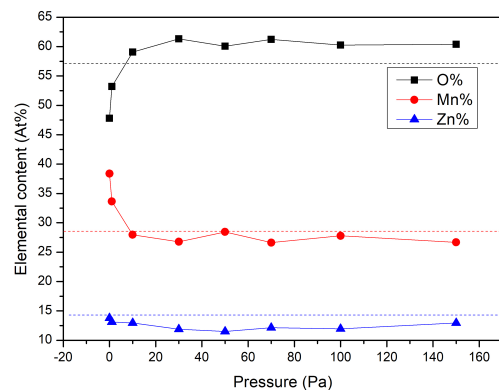

Figure 3: O, Mn, and Zn atomic content in as-deposited ZMO films at different oxygen deposition pressures, as obtained by EDXS measurements. For comparison, dashed lines indicating the theoretical stoichiometry of $ZnMn_2O_4$ are reported.
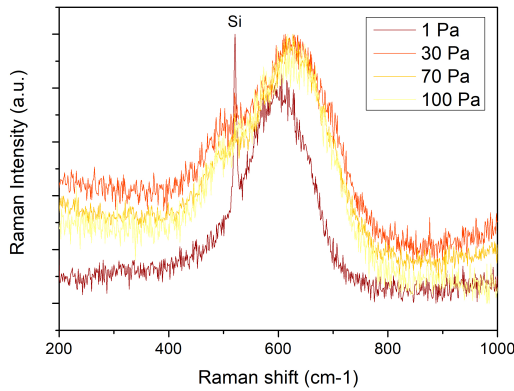
Figure 4: Raman spectra of ZMO films deposited at 1 Pa, 30 Pa, 70 Pa, and 100 Pa of oxygen on silicon substrate (laser wavelength = 660 nm, power = 0.75 mW).
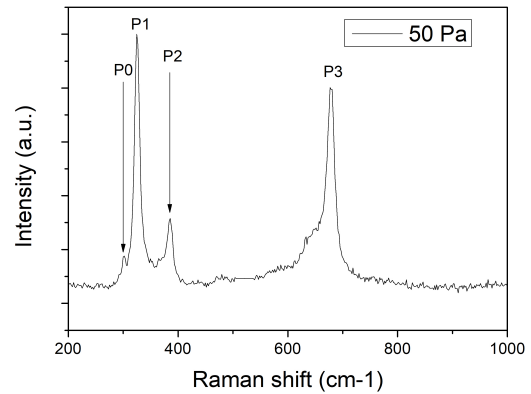

Figure 5: Raman spectrum of ZMO film deposited on FTO-coated glass at 50 Pa of oxygen and annealed in air at 500°C for 2 hours. Excitation laser: $\lambda = 532$ nm, 0.7 mW.

others. Indeed, it is red-shifted, less broad, and does not present a shoulder around 500 cm^{-1} that is present in the other spectra.

4. Crystallization of ZMO films by thermal annealing

As mentioned above, pristine films obtained by PLD are amorphous. Raman spectroscopy was used to check whether the samples, after annealing, are crystalline. In agreement with literature data about Raman spectra of spinel oxides[5], the spectra of annealed ZMO films present four main peaks identified in this work as P0, P1, P2, and P3 (Figure 5). These peaks are always present in my crystallized samples (except for P0 which is sometimes not distinguishable), however, the positions of the peaks, their width, and the intensity ratio between P1 and P3 may vary. I have verified that the minimum annealing temperature for good film crystallization is 500°C, both in air and in vacuum. Selected samples (deposited at 1 Pa and 50 Pa of oxygen on a silicon substrate) were annealed at 500°C, 600°C, 700°C, and 800°C for 2 hours in air and at 500°C for 1 hour in vacuum to investigate the effect of different annealing conditions on the film crystallization. The effect on the film was an increase in crystalline grain size as a function of annealing temperature (with smaller crystals for vacuum annealing at 500°C), visible both in SEM images and in the FWHM reduction of Raman peaks.
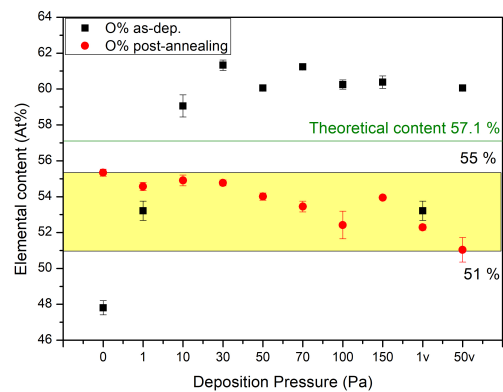

Figure 6: Samples' oxygen content before and after annealing in air or vacuum. The green line indicates the oxygen percent in the stoichiometric $ZnMn_2O_4$ as a reference. 1v and 50v indicate films annealed in vacuum. The error bars are the standard deviations of five measurements taken at different points for each sample.

A study on the effect of deposition oxygen pressure on films subjected to the same heat treatment follows. Moreover, I present a comparison of films deposited under the same conditions before and after annealing. The oxygen content (measured by EDXS) after annealing performed in air at 600°C for 3 h or under vacuum at 500°C for 1 h settles between 51% and 55% regardless the oxygen content in as-deposited films (Figure 6). The morphology of the films changes during
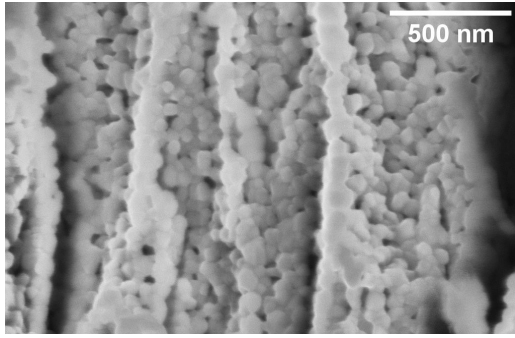
Figure 7: SEM cross-sectional image of the film deposited in 100 Pa of oxygen and annealed in air at 600°C for 3 h.

the annealing process. The first noticeable point is the formation of crystalline grains in the films, which further confirms the crystallization of the material. In the film produced at high pressure of oxygen (e.g., 100 Pa), the cross-sectional SEM images reveal numerous crystals that give rise to a "knotted mesh", where the original tree-like structures are replaced by small crystallites (50-70 nm) arranged into columns (Figure 7). In general, the morphology of annealed films exhibits greater porosity and more voids compared to as-deposited films. The last part of this analysis concerns the influence of different oxygen deposition pressures on the Raman spectra of the annealed films (Figure 8). For the peaks P0, P1, P2, P3, I evaluated the peak positions, FWHMs, and height intensity ratios by fitting the spectra with Lorentzian functions. The result is that films deposited in vacuum or 1 Pa have, in the spectra, different characteristics compared to films deposited at higher oxygen pressure. Moreover, in general, there are differences in the Raman spectra as a function of the oxygen deposition pressure, with an observable shift in peak position and a reverse of the P1/P3 intensity ratio. The first interpretation of these results can be attributed to the effect of crystal size: since different deposition pressures give rise to different crystal sizes and orientations after annealing, the corresponding Raman spectra may reflect this behaviour. However, looking at the obtained trends and comparing them with Nádherný et al. [5]'s work (which analyses the Raman spectra of $Zn_xMn_{3-x}O_4$ samples in which the relative content of Zn and Mn is varied), some similarities can be seen. One may speculate that, the actual Zn/Mn content in the
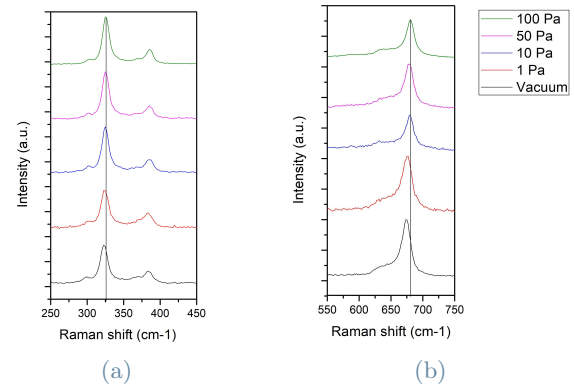

Figure 8: Raman spectra (laser wavelength = 532 nm, power = 0.7 mW) of samples deposited at different oxygen pressures on silicon and annealed at 600°C for 3 h in air. In (a) P0, P1, P2 are visible; in (b) P3 is presented. All the spectra are normalized after removing the signal of the silicon substrate.

crystalline spinel phase is affected by the deposition conditions.

5. Early electrochemical tests on ZMO films

This section presents the preliminary electrochemical measurements and post-electrochemistry Raman analysis performed on selected ZMO samples. The experimental setup employed consisted of a Teflon cell, the ZMO film as the working electrode, one platinum wire as the counter electrode, and one platinum wire as the quasi-reference electrode. The electrolytes adopted for the measurements (∼1 mL) consisted of deionized water with zinc sulfate (2M) and manganese sulfate (0.1M) dissolved (ZMS electrolyte), where $MnSO_4$ additive alleviate the Mn^{2+} dissolution from ZMO film. Finally, the films used for the electrochemical measurements were all produced by PLD at different oxygen pressures on FTO-coated glass substrates and then subjected to annealing in air at 500°C for 2 h. Deposition time at any oxygen pressure was set in order to obtain a film thickness of ∼500-600 nm.

Cyclic voltammetries (CVs) were performed on selected samples with the potential scanning in a range of -0.75 V to +0.75 V vs. Pt-QRef., starting at 0 V, proceeding in cathodic direction, and adopting a scan rate of 25 mV/s
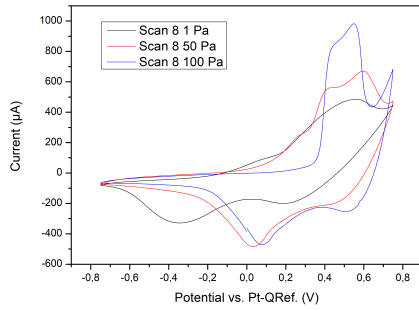
Figure 9: Comparison of the eighth CV cycle performed in ZMS electrolyte on ZMO films deposited on FTO-coated glass at 1 Pa, 50 Pa, and 100 Pa of oxygen and annealed in air at 500°C for 2 h.

for eight cycles. The CVs were performed on samples deposited at 1 Pa, 50 Pa, and 100 Pa of oxygen to test the electrochemical response of films with different porosity. A comparison of the last cycle for each sample is presented in Figure 9. The progression between the three curves is observable, with the film deposited at 1 Pa with only one broad peak in the anodic region, which rises and begins to split at 50 Pa, and, finally, becomes narrower and with two close peaks at 100 Pa. The increase of current before the anodic peak(s) is more gradual for the samples deposited at 1 and 50 Pa of oxygen because of the presence of a shoulder that rises during cycling; instead, a steeper increase is observed for the sample deposited at 100 Pa. Similarly, the cathodic peaks move toward more positive potentials gradually from 1 to 50, to 100 Pa. Morphology (due to different deposition pressures) thus affects charge exchange during electrochemistry, directly influencing the area enclosed in CV curves, peaks height (i.e., current), and reaction kinetics (consequently peaks shape). In conclusion, the CVs obtained from my experiments are consistent with those reported in the literature for ZMO samples[2, 4], especially for the more porous one (100 Pa). They thus demonstrate, despite the study being at an early stage, the compatibility of my films, deposited by PLD, with the electrochemical data reported in the literature for other ZMO nanostructures.

In order to study the evolution of the material during electrochemical polarization, subsequent
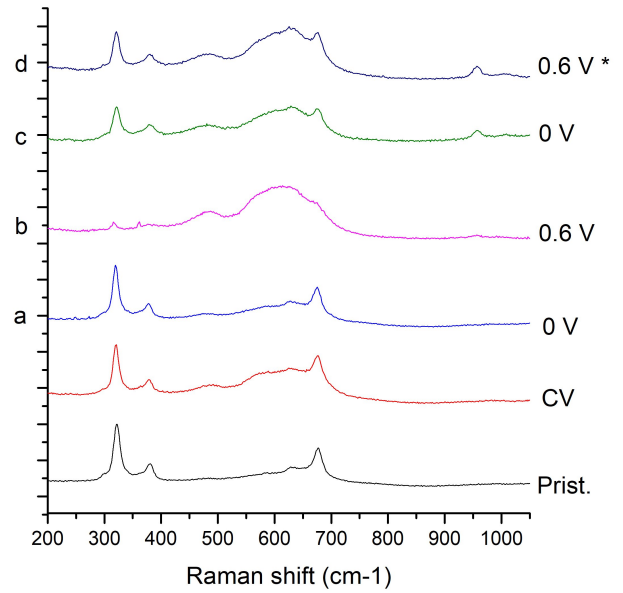
Figure 10: Raman spectra of ZMO film deposited at 100 Pa of oxygen and annealed in air at 500°C for 2 h. Spectra were acquired for pristine ZMO, after the CV, and after four PS tests (a-c in ZMS electrolyte, while d in ZS electrolyte, as indicated by *), applied subsequently on the same sample. Excitation Laser = 532 nm.

constant potentials were applied to the film deposited at 100 Pa and the corresponding Raman spectra were acquired at the end of the potentiostatic (PS) test. The values of the applied potentials were selected according to the CV shown above: +0.6 V was applied to keep the film into the anodic region (oxidation), while the sample was kept at 0 V to promote the reduction. The sample after the first PS at 0 V (cathodic polarization) seems to be more similar to the pristine one, as the P3 peak shoulder lowers (in Figure 10 the spectrum a). The curve representing the current over time shows a negative current tending to 0, confirming that the film is in the cathodic region. After the anodic polarization (+0.6 V, spectrum b in the Figure 10), on the other hand, the two low-frequency peaks P1 and P2 seem to almost disappear, and peak P3 is incorporated in a large band around 600 cm^{-1}. Referring to the article by Yang et al. [2] (which attributes peaks P1 and P2 to Zn-O vibrations), this behaviour could be attributed to the egress of zinc from the material, which results in the fading of the modes associated with it and in the formation

of amorphous manganese dioxide. In fact, in the anodic region the reaction would be:

$$ZnMn_2O_4 \rightarrow Zn^{2+} + 2MnO_2 + 2e^- \qquad (1)$$
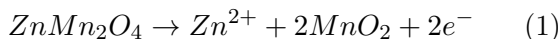
with the oxidation state of manganese changing from Mn^{3+} to Mn^{4+}. The article by Soundharrajan et al. [4] suggests that electrodeposition of manganese dioxide is an important process for electrochemistry in ZMS electrolyte. Actually, the weakening of the zinc-associated modes (P1 and P2) of the material could also be attributed to a covering of the film by electro-deposited manganese dioxide from the Mn^{2+} in the electrolyte and not to the egress of zinc from the ZMO. The third PS (in Figure 10 spectrum c), again in ZMS electrolyte, was performed at 0 V to promote the reduction reaction (to induce the zinc re-intercalate and/or dissolve the electrodeposited MnO_2). As can be seen from the Raman spectrum, the ZMO peaks reappear, although the shoulder associated with P3 still remains significantly more pronounced than that of the pristine material. This latter effect may be due to either amorphization of the material or persistence of MnO_2 irreversibly deposited on the film. Finally, the film was subjected to another oxidation step (+0.6 V, spectrum d in Figure 10), but this time in an electrolyte containing $ZnSO_4$ 2M only (ZS electrolyte), thus eliminating the possibility of manganese dioxide electrodeposition. In this case, the peaks associated with ZMO do not disappear, while the current rapidly drops to zero. The shoulder before P3 increases slightly compared to the previous spectrum, still suggesting a modification of the material.

Some electrochemical tests were performed also on bare FTO-coated glass substrates to evaluate the stability of the substrate itself and the electrodeposition effects of the electrolytes, so as to compare them with the CVs collected on ZMO films. The CVs conducted in different electrolytes are different from each other. CVs in ZS show no electrochemical activity as there is nothing to electrodeposit. Considering the CV due to electrodeposition alone on bare FTO in MnSO4 0.1M (MS electrolyte), it shows differences from both the CV on FTO in ZMS electrolyte and the CVs on ZMO deposited at various pressures. This suggests that the electrochemistry of the material is not due to electrode-

position and dissolution of manganese dioxide alone, otherwise the CVs would all be much more similar. For this reason, I agree with the hypothesis put forward by Soundharrajan et al. [4], who argues that there are three active processes involving ZMO in ZMS electrolyte:

1. Insertion and extraction of Zn^{2+} in the ZMO film;
2. Electrodeposition and dissolution of MnO_x from Mn^{2+} in the electrolyte;
3. Insertion of zinc into electrodeposited MnO_2.

This explains how CVs in ZMS differ from bare FTO and ZMO films, the latter being reactive beyond electrodeposition. It also explains the difference between CVs on bare FTO performed in ZMS and MS electrolytes, as the third mentioned mechanism can only occur in ZMS. In addition, as pointed out by SEM images and Raman/EDXS analyses on the aged sample, zinc hydroxy sulphate hydrate (ZHS) phase was probably formed on the film surface, suggesting the participation of protons in the electrochemical mechanism.

6.   Conclusions

In conclusion, the main objectives have been achieved. I was able to produce via PLD thin films of ZMO by varying the morphology and stoichiometry of the material by depositing them at different oxygen pressures (and in vacuum). It should be stressed that the modification of the morphology and the variation of the stoichiometry of ZMO are two of the possible strategies to increase its electrochemical performances. The characterization of ZMO films produced in an oxygen atmosphere is extensive and covers different experimental conditions for both pristine and annealed films. Finally, the first electrochemical tests, although they need to be extended, have already given useful insights into the mechanisms occurring in the ZMO samples.

References

[1] Niklas Borchers, Simon Clark, Birger Horstmann, Kaushik Jayasayee, Mari Juel, and Philippe Stevens. Innovative zinc-based batteries. *Journal of Power Sources*, 484, 2 2021. ISSN 03787753. doi: 10.1016/j.jpowsour.2020.229309.

[2] Cheng Yang, Meina Han, Huihui Yan, Feng Li, Minjie Shi, and Liping Zhao. In-situ probing phase evolution and electrochemical mechanism of znmn2o4 nanoparticles anchored on porous carbon polyhedrons in high-performance aqueous zn-ion batteries. *Journal of Power Sources*, 452, 3 2020. ISSN 03787753. doi: 10.1016/j.jpowsour.2020.227826.

[3] Kexing Cai, Shao hua Luo, Jie Feng, Jiachen Wang, Yang Zhan, Qing Wang, Yahui Zhang, and Xin Liu. Recent advances on spinel zinc manganate cathode materials for zinc-ion batteries. *Chemical Record*, 22, 1 2022. ISSN 15280691. doi: 10.1002/tcr.202100169.

[4] Vaiyapuri Soundharrajan, Balaji Sambandam, Sungjin Kim, Saiful Islam, Jeonggeun Jo, Seokhun Kim, Vinod Mathew, Yang kook Sun, and Jaekook Kim. The dominant role of mn2+ additive on the electrochemical reaction in znmn2o4 cathode for aqueous zinc-ion batteries. *Energy Storage Materials*, 28: 407–417, 6 2020. ISSN 24058297. doi: 10.1016/j.ensm.2019.12.021.

[5] Ladislav Nádherný, Miroslav Maryško, David Sedmidubský, and Christine Martin. Structural and magnetic properties of znxmn3-xo4 spinels. *Journal of Magnetism and Magnetic Materials*, 413: 89–96, 9 2016. ISSN 03048853. doi: 10.1016/j.jmmm.2016.04.029.